Nano Res (2009) 2: 923–930
DOI 10.1007/s12274-009-9094-8
Research Article

Hydrothermal Synthesis of Orthorhombic $LiMnO_2$ Nanoparticles and $LiMnO_2$ Nanorods and Comparison of their Electrochemical Performances

Xiaoling Xiao[1], Li Wang[2], Dingsheng Wang[1], Xiangming He[2], Qing Peng[1], and Yadong Li[1,3] (✉)

[1] Department of Chemistry, Tsinghua University, Beijing 100084, China
[2] Institute of Nuclear and New Energy Technology, Tsinghua University, Beijing 100084, China
[3] State Key Laboratory of New Ceramics and Fine Processing, Tsinghua University, Beijing 100084, China

Received: 19 August 2009 / Revised: 12 October 2009 / Accepted: 12 October 2009

ABSTRACT

Orthorhombic $LiMnO_2$ nanoparticles and $LiMnO_2$ nanorods have been synthesized by hydrothermal methods. $LiMnO_2$ nanoparticles were synthesized by simple one-step hydrothermal method. To obtain rod-like $LiMnO_2$, γ-MnOOH nanorods were first synthesized and then the H^+ ions were completely replaced by Li^+ resulting in $LiMnO_2$ nanorods. Their electrochemical performances were thoroughly investigated by galvanostatic tests. Although the $LiMnO_2$ nanoparticles have smaller size than $LiMnO_2$ nanorods, the latter exhibited higher discharge capacity and better cyclability. For example, the discharge capacities of $LiMnO_2$ nanorods reached 200 mA·h/g over many cycles and remained above 180 mA·h/g after 30 cycles. However, the maximum capacity of $LiMnO_2$ nanoparticles was only 170 mA·h/g and quickly decreased to 110 mA·h/g after 30 cycles. Nanorods with one-dimensional electronic pathways favor the transport of electrons along the length direction and accommodate volume changes resulting from charge/discharge processes. Thus the morphology of $LiMnO_2$ may play an important role in electrochemical performance.

KEYWORDS

$LiMnO_2$ nanoparticles, nanorods, hydrothermal synthesis, one-dimensional nanomaterial, electrochemical performance

Introduction

Rechargeable Li-ion batteries, as the major kind of portable power source, have been widely used in consumer electronics, mobile phones, and electric vehicles [1–4]. As the performance, price, and safety of Li-ion batteries mainly depend on the properties of the cathode materials, considerable attention has been paid to the search for, and development of, high capacity, cheap and safe cathode materials [5]. $LiCoO_2$, the first commercially successful cathode material for Li-ion batteries, was introduced by the Sony Corporation in 1990 and is still used today. It has a well-ordered layered crystal structure, which is easily prepared and enables a fast and reversible lithium intercalation [6]. However, the high price and

Address correspondence to ydli@mail.tsinghua.edu.cn

toxicity of $LiCoO_2$ have driven researchers to seek alternative materials in recent years. Manganese-based cathodes, including $LiMn_2O_4$ and $LiMnO_2$, are very promising candidates because their price and safety characteristics generally seem to be superior to cobalt or nickel oxides [6]. $LiMn_2O_4$ has been much studied as a cathode material [7–10]. Another candidate, $LiMnO_2$, has a layered structure similar to that of $LiCoO_2$. This structural analogy motivated us to prepare and study its performance as a cathode material. The theoretical discharge capacity of layered $LiMnO_2$ is 285 mA·h/g [11], which is much higher than $LiMn_2O_4$ and $LiCoO_2$. As a result, layered $LiMnO_2$ is of high fundamental and technological interest as a cathode material for rechargeable lithium batteries.

In most previous reports, the synthesis of $LiMnO_2$ involved solid state methods [12–14] or hydrothermal methods [15–18]. Other synthesis methods including sol–gel methods [19], Pechini's route [20], and reverse microemulsion processes [21] have been less widely used. Hydrothermal synthesis is an effective method for preparing nanostructured materials [22, 23]. At the same time, there is growing evidence that nanostructured battery electrode materials show better power performance. The main advantages of nanostructured battery electrode materials included short path lengths for Li transport, the large electrode–electrolyte contact giving higher charge/discharge rates, and better accommodation of the strain thus improving cycle stability [24–26]. Layered $LiMnO_2$ has two main crystal polymorphs, orthorhombic and monoclinic [16]. Since the monoclinic phases is very hard to obtain [27], most studies of layered $LiMnO_2$ have concentrated on the orthorhombic phase, *o*-$LiMnO_2$. So, here, we firstly synthesized orthorhombic $LiMnO_2$ nanoparticles by a one-step hydrothermal method and tested its electrochemical performance. However, the discharge capacity and cyclability of *o*-$LiMnO_2$ nanoparticles were not satisfactory. Subsequently, we synthesized single-crystalline and uniform size γ-MnOOH nanorods, which were transformed into pure-phase *o*-$LiMnO_2$ nanorods in a hydrothermal process. Very interestingly, the $LiMnO_2$ nanorods exhibited higher charge storage capacity and better cycle stability than the $LiMnO_2$ nanoparticles. Although *o*-$LiMnO_2$ nanorods have previously been synthesized and their electrochemical performances investigated [17, 18], in this paper we focus on why the nanorods exhibited better electrochemical performance than the nanoparticles.

1. Experimental

1.1 Synthesis of $LiMnO_2$ nanoparticles

Under stirring, 40 mL of 7.5% H_2O_2 was slowly added to 1.0 g of $MnSO_4$ and 2.4 g of $LiOH{\cdot}H_2O$. The mixed reactants were transferred into an autoclave (50 mL) and heated at 200 °C for 12 h. The system was then allowed to cool to room temperature. The products deposited at the bottom of the vessel. The resulting powder was washed with distilled water several times and subsequently dried at 60 °C.

1.2 Synthesis of γ-MnOOH nanorods

0.7 g of $KMnO_4$ and 0.5 g of cetyltrimethylammonium bromide (CTAB) were dissolved in 40 mL of H_2O. The mixed reactants were transferred into an autoclave (50 mL), sealed, and heated at 180 °C for 12 h. The system was then allowed to cool to room temperature. The resulting powder was washed with ethanol several times and then with distilled water several times, and subsequently dried at 60 °C.

1.3 Synthesis of $LiMnO_2$ nanorods

3.0 g of $LiOH{\cdot}H_2O$ was dissolved in 40 mL of H_2O, and then 0.5 g of the as-prepared γ-MnOOH nanorods were added. After stirring for 10 min, the mixture was transferred into an autoclave (50 mL) and heated at 200 °C for 8 h. The product was washed with distilled water several times and subsequently dried at 60 °C.

1.4 Characterization

The X-ray diffraction (XRD) patterns were collected by using a Rigaku D/max 2500Pc X-ray diffractometer with Cu Kα radiation ($\lambda = 1.5418$ Å). The size and morphology of samples were investigated with a Leo-1530 field-emission scanning electron microscope (FESEM). The powders were

dispersed in ethanol to prepare the SEM samples.

1.5 Electrochemical measurements

The electrochemical properties of the $LiMnO_2$ samples were evaluated using coin type cells with lithium metal as the counter electrode. The working electrode was fabricated by mixing the active material, acetylene black, and polyvinylidene fluoride (PTFE) with a weight ratio 80:10:10. The electrolyte was a 1 mol/L $LiPF_6$ solution in a 1∶1 mixture of ethylene carbonate (EC)/diethyl carbonate (DEC) and the separator was Celgard 2500. The cell was assembled in a glove box filled with highly pure argon gas. The galvanostatic charge/discharge experiments were performed between 2.0 and 4.5 V at different current densities.

2. Results and discussion

2.1 Phase formation and morphology characterization

$LiMnO_2$ nanoparticles were synthesized by a one-step hydrothermal method using $MnSO_4$, LiOH, and H_2O_2. The reaction is believed to take place in three steps. Firstly, $MnSO_4$ and LiOH formed $Mn(OH)_2$ in solution, which was quickly oxidized into $Mn(OH)_3$ by H_2O_2 and air. Then $Mn(OH)_3$ was transformed into $LiMnO_2$ on heating in LiOH solution. The overall process can be expressed as

$$MnSO_4 + LiOH + H_2O_2 \longrightarrow LiMnO_2$$

The XRD pattern of the product (Fig. 1) agreed well with the reported pattern for orthorhombic $LiMnO_2$ (JCPDS 86-0356) except for the peak at 2θ = 18.6° (marked "♦"), which can be attributed to $LiMn_2O_3$.

To obtain rod-like $LiMnO_2$, γ-MnOOH nanorods were first synthesized using CTAB as a reductant for transforming Mn^{7+}($KMnO_4$) into Mn^{3+}, and then the H^+ ions in γ-MnOOH were completely replaced by Li^+ resulting in $LiMnO_2$ nanorods. In the XRD pattern of the precursor (Fig. 2(a)), most reflection peaks can be indexed to monoclinic γ-MnOOH (JCPDS 74-1631). After further hydrothermal treatment in LiOH solution, the γ-MnOOH was completely transformed into $LiMnO_2$ (see Fig. 2(b)). No impurity phase was detected. The chemical reaction can be formulated as

$$\gamma\text{-MnOOH} + LiOH \longrightarrow LiMnO_2 + H_2O$$

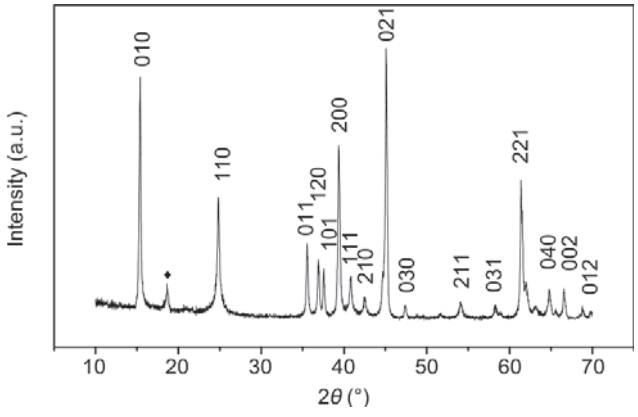

Figure 1 XRD pattern of $LiMnO_2$ nanoparticles prepared from $MnSO_4$

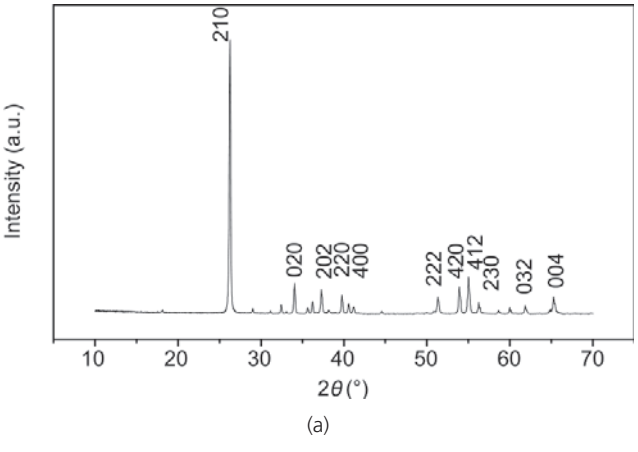

(a)

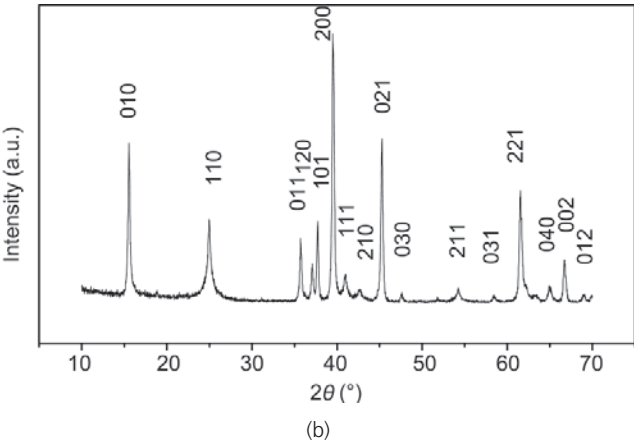

(b)

Figure 2 XRD patterns of γ-MnOOH nanorods (a) and $LiMnO_2$ nanorods (b) prepared from γ-MnOOH

The size and morphology of the samples are shown in Fig. 3. As shown in Fig. 3(a), the $LiMnO_2$ prepared from $MnSO_4$ was composed of nanoparticles, the majority having a size of 20–30 nm with a minority being as large as 200 nm. The SEM image of γ-MnOOH (Fig. 3(b)) shows that the material consisted mainly of uniform nanorod structures with typical diameters in the range 200–300 nm and length of up to tens of micrometers. As shown in Fig. 3 (c), the $LiMnO_2$ prepared from γ-MnOOH retains the rod-like morphology of the precursor even though the reaction was carried out at high temperature and high alkali concentration. An overview SEM image (Fig. 3(c)) shows that the $LiMnO_2$ nanorods were interconnected to form a porous network architecture.

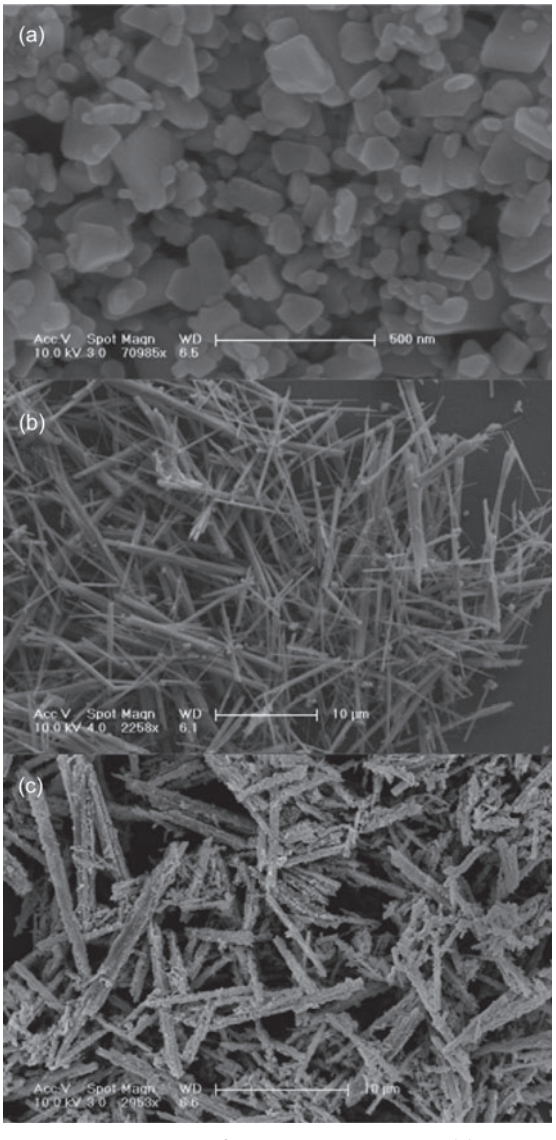

Figure 3 SEM images of $LiMnO_2$ nanoparticles (a), γ-MnOOH nanorods (b), and $LiMnO_2$ nanorods (c)

2.2 Electrochemical performance

The electrochemical performance of as-prepared $LiMnO_2$ nanoparticles and $LiMnO_2$ nanorods were investigated. The discharge curves of $LiMnO_2$ nanoparticles and $LiMnO_2$ nanorods during first five cycles are shown in Figs. 4(a) and 4(b), respectively. The initial discharge curve exhibited a long potential plateau at about 3.0 V (vs. Li^+/Li), which is characteristic of $LiMnO_2$. A plateau of about 4.0 V was observed from the second cycle onwards, which indicates $LiMnO_2$ had transformed into a spinel phase. It has previously been reported [16, 18] that this structural transformation is unavoidable during electrochemical cycling. For both $LiMnO_2$ nanoparticles and $LiMnO_2$ nanorods, the first three cycles involved the activation process and the capacities were lower than the maximum. By only the fourth cycle, however, the discharge capacities reached maximum value. Compared with other materials such as those reported by Zhou et al. [18] requiring 12 cycles, and by Idemoto et al. [13] and Wei et al. [14] requiring as many as 30 cycles, our materials were easy to activate and quickly reached their normal capacities; this can be attributed to the high reaction activity and fast Li-ion transportion of nanosized crystallites. For solid state diffusion of Li in an electrode material, the mean diffusion time (t) can be expressed by the following formula [28]:

$$t = L^2/(2D)$$

where L is the diffusion length, and D is the diffusion coefficient. If we decrease the diffusion length L, through using nanostructured electrode materials, the mean diffusion time (t) will be significantly reduced. Thus, the nanostructured $LiMnO_2$ with its smaller particles and shorter diffusion length gains more momentum and can be activated faster than conventional micrometer-sized materials.

The discharge capacities and cycle stability of $LiMnO_2$ nanoparticles and $LiMnO_2$ nanorods were also compared. Plots of discharge capacities versus cycle number at a rate of 15 mA/g are shown in Fig. 5. The $LiMnO_2$ nanorods clearly

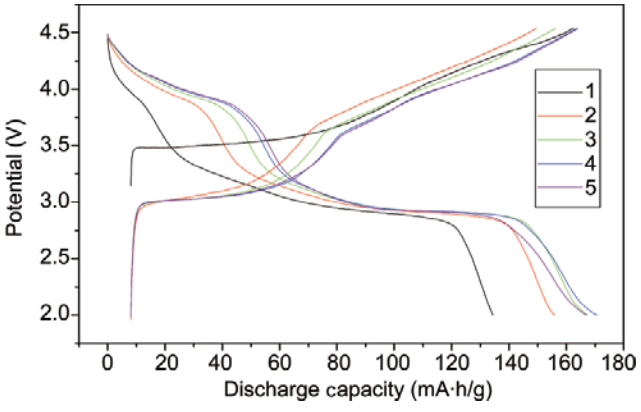

(a)

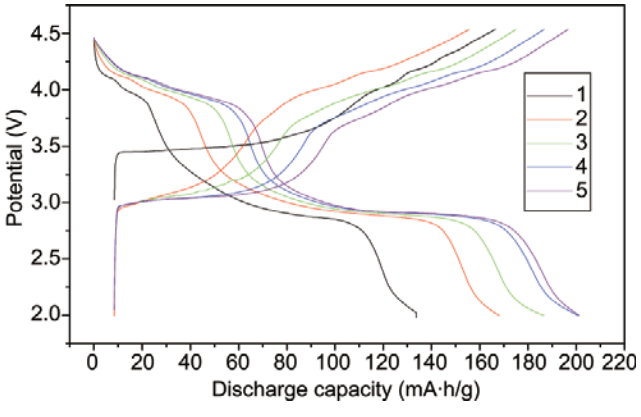

(b)

Figure 4 Charge and discharge curves of $LiMnO_2$ nanoparticles (a) and $LiMnO_2$ nanorods (b) during the first five cycles

exhibited higher discharge capacity and better cyclability than $LiMnO_2$ nanoparticles. The discharge capacities of $LiMnO_2$ nanorods reached about 200 mA·h/g over many cycles and then slowly decreased. After 30 cycles, the discharge capacities still remained above 180 mA·h/g. In contrast, the maximum discharge capacity of $LiMnO_2$ nanoparticles only reached 170 mA·h/g and quickly decreased to 110 mA·h/g after 30 cycles, corresponding to a rapid capacity fading of about 35%. Therefore, the charge/discharge process of the 30th cycle was investigated in detail and the results shown in Fig. 6. In the case of the nanoparticles (Fig. 6(a)), the plateau was tilted and asymmetric. The $LiMnO_2$ nanorods, however, still displayed a long and flat 3.0 V plateau, which suggests that orthohombic $LiMnO_2$ with a rod-like structure is more stable and better able to accommodate volume changes resulting from the

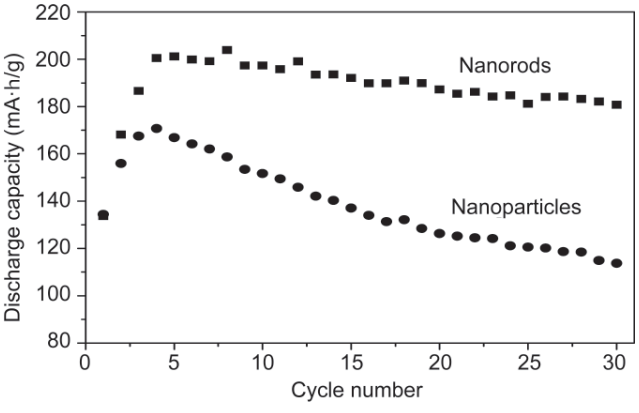

Figure 5 Cycling stability of $LiMnO_2$ nanoparticles (■) and $LiMnO_2$ nanorods (●) at a rate of 15 mA/g

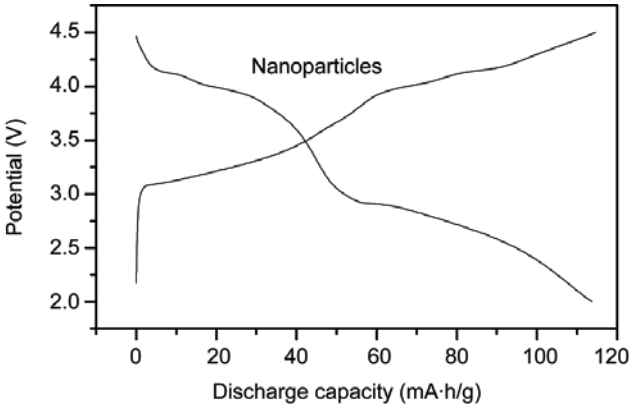

(a)

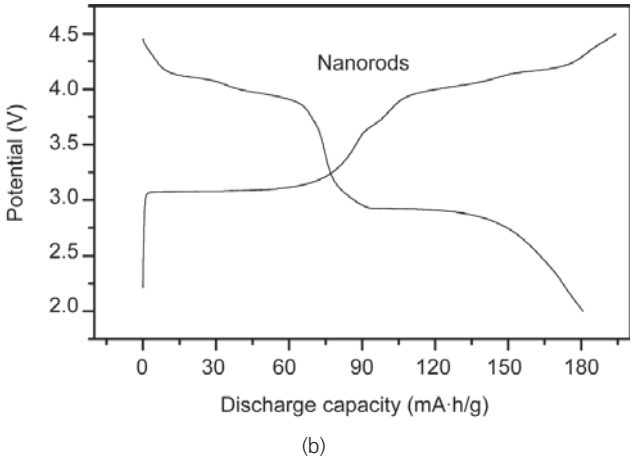

(b)

Figure 6 Charge and discharge curves of $LiMnO_2$ nanoparticles (a) and $LiMnO_2$ nanorods (b) in the 30th cycle

charge/discharge processes.

Though the $LiMnO_2$ nanoparticles had smaller size than the $LiMnO_2$ nanorods, the latter exhibited higher discharge capacity and better cyclability. We conclude that the morphology of $LiMnO_2$ can play an important role in electrochemical performance.

The excellent electrochemical performance of $LiMnO_2$ nanorods results from their one-dimensional nanostructure, which facilitates transport of charge and electrons along the length direction. Furthermore, the one-dimensional nanostructure can provide more reaction sites which accelerate the charge/discharge processes [29]. Previous comparison of many kinds of nanostructured battery electrode materials, including nanoparticles, nanotubes, nanowires, and nanorods, has also demonstrated that one-dimensional nanomaterials like nanowires or nanorods are particularly attractive [26, 30–33]. Cui's group has reported that $LiMn_2O_4$ nanorods have a higher charge storage capacity at high rates compared with commercially available powders [9]. Zhou et al. also reported that $LiMn_2O_4$ nanowires have very high-power density and the discharge capacities at rates of 0.1, 5, 10, and 20 A/g reached 118, 108, 102, and 88 mA·h/g, respectively [10]. In addition, as observed by scanning electron microscopy (SEM) (Fig. 3(c)), the $LiMnO_2$ nanorods have an interdigitated space distribution, which helps to diffuse the electrolyte and also reduces the stress resulting from the charge/discharge process, which in turn, suppresses the loss of discharge capacity. A similar phenomenon has been observed by Chen's group [34].

In terms of their practical application as cathode electrodes in rechargeable lithium batteries, the rate capability of materials is particularly important [35]. Since the $LiMnO_2$ nanorods displayed high discharge capacities and good cycle stability, their rate capability was also investigated. The discharge capacities as a function of discharge rates at 20, 40, 100, and 200 mA/g were evaluated and are shown in Fig. 7, where the charge/discharge cycle was carried out 10 times at every rate. On the whole, the discharge capacity decreased significantly with increasing discharge rate. At low discharge rates, like 20 and 40 mA/g, the discharge capacity and the cyclability were close to ideal and the discharge capacity approached 170 mA·h/g at a rate of 40 mA/g. However, when discharge rate was increased to 100 or 200 mA/g, the discharge capacity was significantly reduced and the cyclability became worse. The capacities only reached 90 mA·h/g at a rate of 200 mA/g, which was only half of the discharge capacity at a rate of 20 mA/g. Similar results, with a discharge capacity of about 90 mA·h/g observed at a discharge rate of 1 h (1 C), were reported by Ammundsen who commented that the loss of capacity at higher discharge rates is a problem for practical applications [6]. Our results also showed that the reduction of capacity at higher discharge rates was serious. Therefore, we suggest that for practical applications, orthorhombic $LiMnO_2$ may be more suitable for systems with smaller charge/discharge rates.

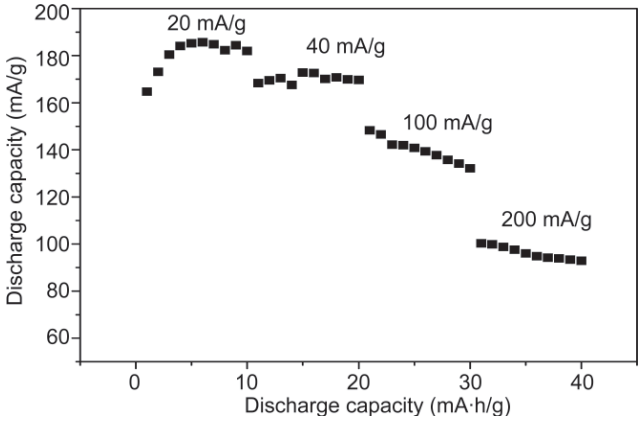

Figure 7 Plots of discharge capacity vs. number of cycles for $LiMnO_2$ nanorods at different rates

3. Conclusions

Orthorhombic $LiMnO_2$ nanoparticles and $LiMnO_2$ nanorods have been synthesized by a one-step hydrothermal method and a two-step hydrothermal method, respectively. $LiMnO_2$ nanorods displayed a superior electrochemical performance to that of the $LiMnO_2$ nanoparticles, with higher discharge capacity and better cyclability. This suggests that the morphology of $LiMnO_2$ plays an important role in its electrochemical performance. Nanorods with one-dimensional electronic pathways facilitate charge and electron transport, and could potentially improve the electrode-filled ratio. We believe that one-dimensional nanostructured materials have great potential applications in the battery electrode materials area. A study of rate capability indicated that orthorhombic $LiMnO_2$ may be more suitable for systems with smaller charge/discharge rates.

Acknowledgements

This work was supported by the National Natural Science Foundation of China (No. 90606006), and the State Key Project of Fundamental Research for Nanoscience and Nanotechnology (No. 2006CB932300).

References

[1] Tarascon, J. M.; Armand, M. Issues and challenges facing rechargeable lithium batteries. *Nature* **2001**, *414*, 359–367.

[2] Luo, J. Y.; Xia, Y. Y. Aqueous lithium-ion battery $LiTi_2(PO_4)_3/LiMn_2O_4$ with high power and energy densities as well as superior cycling stability. *Adv. Funct. Mater.* **2007**, *17,* 3877–3884.

[3] Aricò, A. S.; Bruce, P.; Scrosati, B.; Tarascon, J. -M.; van Schalkwijk, W. Nanostructured materials for advanced energy conversion and storage devices. *Nat. Mater.* **2005**, *4,* 366–377.

[4] Okubo, M.; Hosono, E.; Kim, J.; Enomoto, M.; Kojima, N.; Kudo, T.; Zhou, H.; Honma, I. Nanosize effect on high-rate Li-ion intercalation in $LiCoO_2$ electrode. *J. Am. Chem. Soc.* **2007**, *129,* 7444–7452.

[5] Lu, Z. H.; MacNeil, D. D.; Dahn, J. R. Layered $Li[Ni_xCo_{1-2x}Mn_x]O_2$ cathode materials for lithium-ion batteries. *Electrochem. Solid-State Lett.* **2001**, *4,* A200–A203.

[6] Ammunden, B.; Paulsen, J. Novel lithium-ion cathode materials based on layered manganese oxides. *Adv. Mater.* **2001**, *13,* 943–956.

[7] Shaju, K. M.; Bruce, P. G. A stoichiometric nano-$LiMn_2O_4$ spinel electrode exhibiting high power and stable cycling. *Chem. Mater.* **2008**, *20,* 5557–5562.

[8] Cho, J. VO_x-coated $LiMn_2O_4$ nanorod clusters for lithium battery cathode materials. *J. Mater. Chem.* **2008**, *18,* 2257–2261.

[9] Kim, D. K.; Muralidharan, P.; Lee, H. -W.; Ruffo, R.; Yang, Y.; Chan, C. K.; Peng, H.; Huggins, R. A.; Cui. Y. Spinel $LiMn_2O_4$ nanorods as lithium ion battery cathodes. *Nano Lett.* **2008**, *8,* 3948–3952.

[10] Hosono, E.; Kudo, T.; Honma, I.; Matsuda, H.; Zhou, H. Synthesis of single crystalline spinel $LiMn_2O_4$ nanowires for a lithium ion battery with high power density. *Nano Lett.* **2009**, *9,* 1045–1051.

[11] Amundsen, B.; Desilvestro, J.; Groutso, T.; Hassell, D.; Metson, J. B.; Regan, E.; Steiner, R.; Pickering, P. J. Formation and structural properties of layered $LiMnO_2$ cathode materials. *J. Electrochem. Soc.* **2000**, *147,* 4078–4082.

[12] Lee, Y. S.; Sun, Y. K.; Adachi, K.; Yoshio, M. Synthesis and electrochemical characterization of orthorhombic $LiMnO_2$ material. *Electrochim. Acta* **2003**, *48,* 1031–1039.

[13] Idemoto, Y.; Mochizuki, T.; Ui, K.; Koura, N. Properties, crystal structure, and performance of *o*-$LiMnO_2$ as cathode material for Li secondary batteries. *J. Electrochem. Soc.* **2006**, *153,* A418–A424.

[14] Wei, Y. J.; Ehrenberg, H.; Bramnik, N. N.; Nikolowski, K.; Baehtz, C.; Fuess, H. *In situ* synchrotron diffraction study of high temperature prepared orthorhombic $LiMnO_2$. *Solid State Ionics* **2007**, *178,* 253–257.

[15] Wu, M. Q.; Zhang, Q. Y.; Lu, H. P.; Chen, A. Nanocrystalline orthorhombic $LiMnO_2$ cathode materials synthesized by a two-step liquid-phase thermal process. *Solid State Ionics* **2004**, *169,* 47–50.

[16] Liu, Q.; Li, Y. X.; Hu, Z. L.; Mao, D. L.; Chang, C. K.; Huang, F. Q. One-step hydrothermal routine for pure-phased orthorhombic $LiMnO_2$ for Li ion battery application. *Electrochim. Acta* **2008**, *53,* 7298–7302.

[17] Liu, Q.; Mao, D. L.; Chang, C. K.; Huang, F. Q. Phase conversion and morphology evolution during hydrothermal preparation of orthorhombic $LiMnO_2$ nanorods for lithium ion battery application. *J. Power Sources* **2007**, *173,* 538–544.

[18] Zhou, F.; Zhao, X. M.; Liu, Y. Q.; Li, L.; Yuan, C. G. Size-controlled hydrothermal synthesis and electrochemical behavior of orthorhombic $LiMnO_2$ nanorods. *J. Phys. Chem. Solids* **2008**, *69,* 2061–2065.

[19] Guo, Z. P.; Konstantinov, K.; Wang, G. X.; Liu, H. K.; Dou, S. X. Preparation of orthorhornbic $LiMnO_2$ material via the sol–gel process. *J. Power Sources* **2003**, *119,* 221–225.

[20] Wu, S. H.; Yu, M. Preparation and characterization of *o*-$LiMnO_2$ cathode materials. *J. Power Sources* **2007**, *165,* 660–665.

[21] Lu, C. H.; Wang, H. C. Reverse-microemulsion preparation and characterization of ultrafine orthorhombic $LiMnO_2$ powders for lithium-ion secondary batteries. *J. Eur. Ceram. Soc.* **2004**, *24,* 717–723.

[22] Feng, S. H.; Xu, R. R. New materials in hydrothermal synthesis. *Acc. Chem. Res.* **2001**, *34,* 239–247.

[23] Wang, X.; Zhuang, J.; Peng, Q.; Li, Y. D. A general strategy for nanocrystal synthesis. *Nature* **2005**, *437,* 121–124.

[24] Cheng, F. Y.; Tao, Z. L.; Liang, J.; Chen, J. Template-directed materials for rechargeable lithium-ion batteries. *Chem. Mater.* **2008**, *20,* 667–681.

[25] Kim, M. G.; Cho, J. Reversible and high-capacity nanostructured electrode materials for Li-ion batteries. *Adv. Funct. Mater.* **2009**, *19,* 1497–1514.

[26] Li, Y. G.; Tan, B.; Wu, Y. Y. Mesoporous Co_3O_4 nanowire arrays for lithium ion batteries with high capacity and rate capability. *Nano Lett.* **2008**, *8,* 265–270.

[27] Jang, Y. I.; Moorehead, W. D.; Chiang, Y. M.; Synthesis of the monoclinic and orthorhombic phases of $LiMnO_2$ in oxidizing atmosphere. *Solid State Ionics* **2002**, *149,* 201–207.

[28] Guo, Y. G.; Hu, J .S.; Wan, L. J. Nanostructured materials for electrochemical energy conversion and storage devices. *Adv. Mater.* **2008**, *20,* 2878–2887.

[29] Park, M. S.; Wang, G. X.; Kang, Y. K.; Wexler, D.; Dou, S. X.; Liu, H. K. Preparation and electrochemical properties of SnO_2 nanowires for application in lithium-ion batteries. *Angew. Chem. Int. Edit.* **2007**, *46,* 750–753.

[30] Park, M. S.; Kang, Y. M.; Wang, G. X.; Dou, S. X.; Liu, H. K. The effect of morphological modification on the electrochemical properties of SnO_2 nanomaterials. *Adv. Funct. Mater.* **2008**, *18,* 455–461.

[31] Chan, C. K.; Zhang, X. F.; Cui, Y. High capacity Li ion battery anodes using Ge nanowires. *Nano Lett.* **2008**, *8,* 307–309.

[32] Niu, Z. W.; Bruchman, M. A.; Harp, B.; Mello, C. M.; Wang, Q. Bacteriophage M13 as a scaffold for preparing conductive polymeric composite fibers. *Nano Res.* **2008**, *1,* 235–241.

[33] Li, Y. G.; Wu, Y. Y. Formation of $Na_{0.44}MnO_2$ nanowires via stress-induced splitting of birnessite nanosheets. *Nano Res.* **2009**, *2,* 54–60.

[34] Ma, H.; Zhang, S. Y.; Ji, W. Q.; Tao, Z. L.; Chen, J. α-CuV_2O_6 nanowires: Hydrothermal synthesis and primary lithium battery application. *J. Am. Chem. Soc.* **2008**, *130,* 5361–5367.

[35] Armstrong, A. R.; Paterson, A. J.; Robertson, A. D.; Bruce, P. G. Nonstoichiometric layered $Li_xMn_yO_2$ with a high capacity for lithium intercalation/deintercalation. *Chem. Mater.* **2002**, *14,* 710–719.